

How many extra-Galactic stellar-mass binary black holes will be detected by space gravitational-wave interferometers?

Naoki Seto¹ and Koutarou Kyutoku^{1,2,3}

¹*Department of Physics, Kyoto University, Kyoto 606-8502, Japan*

²*Center for Gravitational Physics, Yukawa Institute for Theoretical Physics, Kyoto University, Kyoto 606-8502, Japan*

³*Interdisciplinary Theoretical and Mathematical Sciences Program (iTHEMS), RIKEN, Wako, Saitama 351-0198, Japan*

11 January 2022

ABSTRACT

On the basis of GWTC-3, we discuss the detection prospect of extra-Galactic binary black holes (BBHs) by space gravitational-wave interferometers. In particular, targeting BBHs with component masses around 5–100 M_{\odot} , we directly incorporate the chirp mass distribution of the 62 BBHs detected at high significance. We find that, due to the reduction of both the comoving merger rate and a weighted average of chirp masses, the expected detection numbers are generally much smaller than the results obtained by the same authors immediately after the report of GW150914. For LISA, the total BBH detections are estimated to be $N_{\text{tot}} \sim 2(T/4\text{yr})^{3/2}(\rho_{\text{thr}}/10)^{-3}$, dominated by nearly monochromatic BBHs (ρ_{thr} : the detection threshold, T : the observational period). TianQin will have a total detection number N_{tot} similar to LISA. Meanwhile, TianQin has potential to find $N_{\text{mer}} \sim 0.6(T/4\text{yr})^{7/4}(\rho_{\text{thr}}/10)^{-3}$ BBHs that merge in the observational period. This number for merging BBHs is 4–5 times larger than that of LISA, because of the difference between the optimal bands. We also investigate prospects for joint operations of multiple detectors, finding that concurrent observations will be more advantageous than sequential ones.

Key words: gravitational waves — binaries: close

1 INTRODUCTION

Since the discovery of the first event GW150914, Advanced LIGO and Advanced Virgo have observed mergers of ~ 80 binary black holes (BBHs), as recently summarized in the catalog GWTC-3 (Abbott et al. 2021a). The large number of samples allows us to examine various astronomical properties such as the mass distribution of BBHs, the comoving merger rate and its redshift dependence (Abbott et al. 2021b).

BBHs are interesting observational targets also for space interferometers such as LISA (Amaro-Seoane et al. 2017). The detection prospects by these future detectors can be evaluated by combining astrophysical as well as instrumental information (noise curve, operation period etc.). In 2016, shortly after the announcement of GW150914 (Abbott et al. 2016), the authors studied the expected number of BBH detections with LISA (Kyutoku & Seto 2016, paper 1, see also Sesana 2016; Del Pozzo, Sesana, & Klein 2018; Liu et al. 2020). In the past 6 years after the study, along with the significant improvement in our knowledge on BBHs, the sensitivity goal of LISA was refined and narrowed down.

Furthermore, two Chinese missions, TianQin and Taiji have been actively developed (Luo et al. 2016; Ruan et al. 2018). Therefore, comparing with paper 1, we can now draw a more precise picture about the prospects of the BBH observation with space interferometers.

In this paper, by using GWTC-3, we estimate the total numbers of BBH detections with LISA and TianQin. To this end, we directly leverage the mass distribution of the 62 BBHs detected so far at high significance level. We also evaluate the numbers of BBHs that merge in operation periods of the detectors. The latter would be important for multi-band observations (see e.g., Sesana 2016; Nair, Jhingan & Tanaka 2016; Isoyama, Nakano & Nakamura 2018). We find that, due to reduction of both the comoving merger rate and the weighted averaged of chirp masses, the expected numbers of BBH detections become much smaller than the typical values presented in paper 1.

This paper is organized as follows. In §2, from GWTC-3, we extract information of BBHs relevant to this paper. In §3, we review the formulation in paper 1 for calculating the detectable comoving volume. In §4, we evaluate the

arXiv:2201.02766v1 [astro-ph.HE] 8 Jan 2022

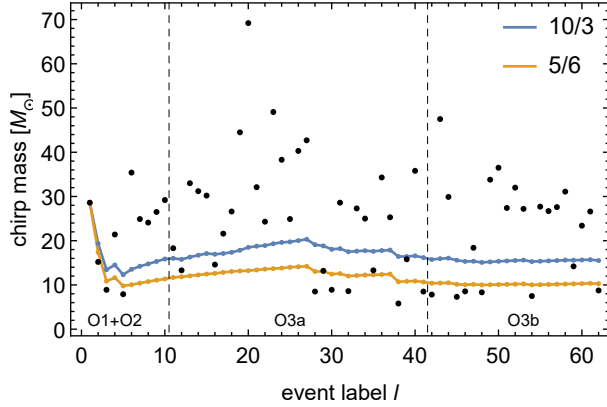


Figure 1. Observed (median) chirp masses \mathcal{M}_l (black dots) and the averaged ones $\bar{\mathcal{M}}_\alpha$ with $\alpha = 10/3$ and $5/6$. The total number of BBHs is 62 labelled by l in the chronological order (O1: 3, O2: 7, O3a: 31 and O3b : 21 events). The weighted average of the chirp masses $\bar{\mathcal{M}}_\alpha$ were evaluated by using the first l events with Eq. (11).

detectable numbers, using a simplified model and a mass-weighted model. We also discuss the impacts of the joint operation of two space interferometers such as the LISA-TianQin pair. In §5, we make a brief discussion on possible modifications to our results. §6 is devoted to a summary of this paper.

2 CHIRP MASS DISTRIBUTION

In Fig. 1, with the black dots, we show the observed (median) chirp masses \mathcal{M}_l (in the source frame) for the 62 BBHs reported in GWTC-3 with the false alarm rates (FARs) lower than 0.25yr^{-1} (Abbott et al. 2021b). For each event, we chronologically assign the label l with $l = 1$ for GW150914 and $l = 62$ for GW200316.21576. The maximum value $\mathcal{M}_{20} = 69.2M_\odot$ is for GW190521.030229. We also show the beginnings of the O3a and O3b runs. Following Abbott et al. (2021b), we exclude the outlier GW190814 from our sample (closely related to the argument about the lower mass gap). Therefore, we study BBHs with component masses in the range $[5M_\odot, 100M_\odot]$ and the chirp masses around $[5M_\odot, 70M_\odot]$.

Abbott et al. (2021b) estimated the comoving merger rate of BBHs in the range $17.3\text{--}45\text{Gpc}^{-3}\text{yr}^{-1}$ at the redshift $z = 0.2$ with the fitted dependence $(1+z)^\kappa$ ($\kappa = 2.7_{-1.9}^{+1.8}$). Since LISA can only observe stellar mass BBHs at lower redshifts than current ground-based detectors, we estimate the mean rate at $z = 0$ by

$$R_0 = (17.3 + 45)/2 \times (1 + 0.2)^{-2.7} = 19.1\text{Gpc}^{-3}\text{yr}^{-1}, \quad (1)$$

expecting an uncertainty factor of two (see Fig. 13 in Abbott et al. 2021b).

Next, we discuss the chirp mass distribution function $P(\mathcal{M})$ for the comoving merger rate, using the observed 62 chirp masses. We impose the normalization

$$\int_{\mathcal{M}_{\min}}^{\mathcal{M}_{\max}} d\mathcal{M}P(\mathcal{M}) = 1 \quad (2)$$

in the mass range $[\mathcal{M}_{\min}, \mathcal{M}_{\max}]$. In concrete terms, we simply assume that (i) a BBH can be detected if and only if its

signal-to-noise ratio exceeds a certain threshold, and (ii) the signal-to-noise ratio is dominated by the inspiral waveform ($\propto \mathcal{M}^{5/6}/D$ with the distance D). Then, ignoring the cosmological effects, the detectable volume is $\propto D^3 \propto \mathcal{M}^{5/2}$.

For the sake of conceptual convenience for dealing with the probability measure, we temporarily divide the chirp masses into finite segments with the labels $\sigma = 1, \dots, \sigma_{\max}$. We put $\Delta\mathcal{M}_\sigma$ and \mathcal{M}_σ for the width and the central value for the segment σ (with $\mathcal{M}_{\sigma=1} \sim \mathcal{M}_{\min}$ and $\mathcal{M}_{\sigma=\sigma_{\max}} \sim \mathcal{M}_{\max}$). Our final results do not depend on the detail of the segmentation.

For a segment σ , the expected detection number is given by

$$n_\sigma = KP(\mathcal{M}_\sigma)\Delta\mathcal{M}_\sigma\mathcal{M}_\sigma^{5/2} \quad (3)$$

with the factor K independent of the segment. We then have

$$P(\mathcal{M}_\sigma)\Delta\mathcal{M}_\sigma = K^{-1}n_\sigma\mathcal{M}_\sigma^{-5/2} \quad (4)$$

or

$$P(\mathcal{M}_\sigma)\Delta\mathcal{M}_\sigma = \frac{n_\sigma\mathcal{M}_\sigma^{-5/2}}{\sum_{\sigma=1}^{\sigma_{\max}} n_\sigma\mathcal{M}_\sigma^{-5/2}}, \quad (5)$$

taking into account the normalization.

Now we can approximately take the statistical average with respect to the probability distribution $P(\mathcal{M})$. We can formally write down the weighted value of a function $g(\mathcal{M})$ by

$$\langle g(\mathcal{M}) \rangle = \int_{\mathcal{M}_{\min}}^{\mathcal{M}_{\max}} g(\mathcal{M})P(\mathcal{M})d\mathcal{M}. \quad (6)$$

Using the segmentation, we have

$$\langle g(\mathcal{M}) \rangle \simeq \sum_{\sigma=1}^{\sigma_{\max}} g(\mathcal{M}_\sigma)P(\mathcal{M}_\sigma)\Delta\mathcal{M}_\sigma \quad (7)$$

$$\simeq \frac{\sum_{\sigma} g(\mathcal{M}_\sigma)n_\sigma\mathcal{M}_\sigma^{5/2}}{\sum_{\sigma} n_\sigma\mathcal{M}_\sigma^{-5/2}} \quad (8)$$

$$\simeq \frac{\sum_l g(\mathcal{M}_l)\mathcal{M}_l^{-5/2}}{\sum_l \mathcal{M}_l^{-5/2}}. \quad (9)$$

In Eq. (9), we replace the segment label σ by the event label l . This expression is independent of the segmentation.

As an example, we define the mean chirp mass with the power index α by

$$\bar{\mathcal{M}}_\alpha \equiv \langle \mathcal{M}^\alpha \rangle^{1/\alpha} \quad (10)$$

$$= \left(\frac{\sum_l \mathcal{M}_l^{\alpha-5/2}}{\sum_l \mathcal{M}_l^{-5/2}} \right)^{1/\alpha}. \quad (11)$$

For our analysis below, the weighted average of the chirp masses $\bar{\mathcal{M}}_{10/3}$ is particularly important, as explained later with Eq. (28). In Fig. 1, together with $\bar{\mathcal{M}}_{5/6}$ (see §4.2), we show $\bar{\mathcal{M}}_{10/3}$ obtained by using the first l events in Eq. (9). At the right end ($l = 62$), we have $\bar{\mathcal{M}}_{10/3} = 15.5M_\odot$ and $\bar{\mathcal{M}}_{5/6} = 10.3M_\odot$ ($\sim 4\%$ smaller than the results at $l = 41$ corresponding to the end of O3a). In addition to the 62 BBHs with $\text{FAR} < 0.25\text{yr}^{-1}$, Abbott et al. (2021b) provided seven more BBHs with $0.25\text{yr}^{-1} < \text{FAR} < 1\text{yr}^{-1}$ (excluding GW190917). Even using 69 BBHs, the two weighted averages of the masses $\bar{\mathcal{M}}_{10/3}$ and $\bar{\mathcal{M}}_{5/6}$ change only by $\sim 1\%$.

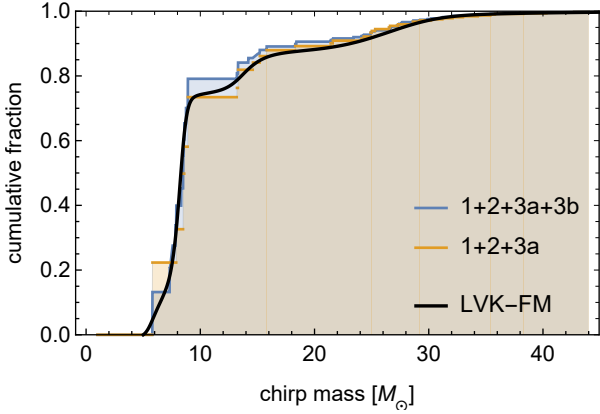


Figure 2. The cumulative chrip mass distributions of BBHs for the comoving merger rate. The orange steps are the result from the 41 BBHs in O1+O2+O3a and the blue steps are from the 62 BBHs in O1+O2+O3a+O3b. The black curve is a model prediction in Abbott et al. (2021b).

We can also evaluate the cumulative chrip mass distribution by

$$P(< \mathcal{M}_{\text{thr}}) \equiv \int_{\mathcal{M}_{\text{min}}}^{\mathcal{M}_{\text{thr}}} P(\mathcal{M}) d\mathcal{M} = \langle \theta(\mathcal{M}_{\text{thr}} - \mathcal{M}) \rangle. \quad (12)$$

In Fig. 2, we present the numerical results obtained by using all the 62 events (from O1, O2, O3a and O3b) and the 41 events excluding O3b. We can clearly see the deficiency in the range 9-13 M_{\odot} . We comment that, in contrast to the original distribution $P(\mathcal{M})$, the appearance of the cumulative distribution $P(< \mathcal{M}_{\text{thr}})$ is less affected by the smoothing operation associated with the discreteness of the samples.

Abbott et al. (2021b) provided an estimate for the function $P(\mathcal{M})$, based on the flexible mixture (FM) model framework¹. In Fig. 2, we present its cumulative profile that shows a reasonable agreement with our results. Using their distribution function, we also evaluated the mean chrip masses, and obtained $\bar{\mathcal{M}}_{10/3} = 16.4M_{\odot}$ and $\bar{\mathcal{M}}_{5/6} = 10.8M_{\odot}$. These numerical values are larger only by $\sim 5\%$ than our simple evaluations.

In the analysis below, we use the comoving merger rate $R_0 = 19.1\text{Gpc}^{-3}\text{yr}^{-1}$ at $z = 0$ and the direct averaging (9) with the 62 BBH samples in the range $[\mathcal{M}_{\text{min}}, \mathcal{M}_{\text{max}}] = [5M_{\odot}, 70M_{\odot}]$, resulting in $\bar{\mathcal{M}}_{10/3} = 15.5M_{\odot}$. In paper 1, we used the BBH merger rate $R = 100\text{Gpc}^{-3}\text{yr}^{-1}$, assuming the single mass profile at $\mathcal{M} = 28.6M_{\odot}$, mainly based on the first event GW150914 (Abbott et al. 2016). These values are much larger than the updated ones in this paper.

3 EVOLUTION OF INDIVIDUAL BINARY BLACK HOLES

In this section, following paper 1, we briefly summarize evolution of a circular BBH initially at a frequency f_i , and discuss detection of its GWs with space interferometers.

From the quadrupole formula, the chrip rate of its GW

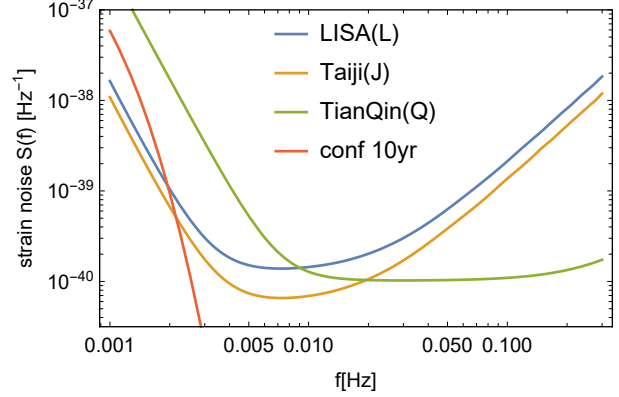


Figure 3. The angular averaged strain noise spectra $S(f)$ for LISA, Taiji and TianQin. The Galactic confusion noise is given for $T = 10\text{yr}$.

frequency is given by

$$\frac{df}{dt} = \frac{96\pi^{8/3}G^{5/3}\mathcal{M}^{5/3}f^{11/3}}{5c^5}. \quad (13)$$

By integrating this equation, the remaining time before the merger is estimated to be

$$t_{\text{mer}} = \frac{5c^5 f_i^{-8/3}}{256\pi^{8/3}G^{5/3}\mathcal{M}^{5/3}} \quad (14)$$

$$= 4\text{yr} \left(\frac{f_i}{25\text{mHz}} \right)^{-8/3} \left(\frac{\mathcal{M}}{15.5M_{\odot}} \right)^{-5/3}. \quad (15)$$

Similarly, after an observational period T less than t_{mer} , the final frequency f_f is written by

$$f_f(f_i, T) = f_i \left(\frac{t_{\text{mer}} - T}{t_{\text{mer}}} \right)^{-3/8}. \quad (16)$$

For $T > t_{\text{mer}}$, we should formally put $f_f = \infty$ in our analysis below.

The signal-to-noise ratio ρ is given by

$$\rho^2 = 4 \int_{f_i}^{f_f} \frac{|\tilde{h}(f)|^2}{(3/20)S(f)} df \quad (17)$$

with the Fourier transformed amplitude $|\tilde{h}(f)|$ and the angular averaged noise spectrum $S(f)$ for a triangular detector unit. In Fig. 3, we show the target sensitivity $S(f)$ for LISA (Robson, Cornish, & Liu 2019), Taiji (Wang et al. 2020) and TianQin (Huang et al. 2020), along with the Galactic confusion noise for $T = 10\text{yr}$ (Robson, Cornish, & Liu 2019). For LISA with the armlength of 2.5Gm, the A- and E-channels can be regarded as the main data streams for BBH detection at $f \lesssim 30\text{mHz}$ (Prince et al. 2002).

At the quadrupole order, the GW amplitude is expressed as

$$|\tilde{h}(f)|^2 = \frac{5G^{5/3}\mathcal{M}^{5/3}}{24\pi^{4/3}c^3D^2f^{7/3}} \times \frac{3}{4} \left[F_+^2 \left(\frac{1+\mu^2}{2} \right)^2 + F_{\times}^2 \mu^2 \right] \quad (18)$$

with the distance D and $\mu \equiv \cos I$ (I : the inclination angle). The beam pattern functions $F_{+, \times}$ are defined for a triangular unit and normalized appropriately (in relation to the noise spectrum $S(f)$). They are generally time dependent. However, for LISA and Taiji, due to the annual rotation of

¹ <https://zenodo.org/record/5655785#.YdP0n9tUu0q>

their detector planes, we can replace them relatively accurately by their angular averages $\langle F_+^2 \rangle_a = \langle F_\times^2 \rangle_a = 1/5$, at least for $t_{\text{mer}} > T > 2\text{yr}$ (see e.g., Robson et al. 2019).

Then, for a given threshold ρ_{thr} of the signal-to-noise ratio, the effective volume of the BBH detection is estimated to be

$$V(f_i, T) = \frac{4\pi}{3} \times U \frac{A^3}{\rho_{\text{thr}}^3} I_7(f_i, T)^{3/2}. \quad (19)$$

Here, we put

$$I_7(f_i, T) \equiv \int_{f_i}^{f_f} \frac{f^{-7/3}}{(3/20)S(f)} df \quad (20)$$

$$A \equiv \frac{G^{5/6} \mathcal{M}^{5/6}}{2^{3/2} \pi^{2/3} c^{3/2}} \quad (21)$$

and define

$$U \equiv \frac{1}{2} \int_{-1}^1 \left[\left(\frac{1+\mu^2}{2} \right)^2 + \mu^2 \right]^{3/2} d\mu = 0.822 \quad (22)$$

for the inclination $\mu = \cos I$. In this paper, unless otherwise stated, we put $\rho_{\text{thr}} = 10$ (see also §5). In Fig. 3, around the optimal frequency band, the noise spectrum $S(f)$ of Taiji is ~ 2 times smaller than that of LISA. Therefore, the detectable volume of Taiji is $2^{3/2} \sim 3$ times larger.

In fact, the detector plane of TianQin will be always normal to the direction of a white dwarf binary RX J0806.3+1527 (Luo et al. 2016). Then, the averaging for the beam pattern functions does not work as in the case of LISA and Taiji. Using the prescription for the separation of the direction and orientation angles (Seto 2014), this difference increases the detectable volume of TianQin approximately by a factor of

$$\frac{\langle (F_+^2 + F_\times^2)^{3/2} \rangle_a}{\langle F_+^2 + F_\times^2 \rangle_a^{3/2}} \approx \frac{U}{(4/5)^{3/2}} = 1.15. \quad (23)$$

In order to include this correction, in Fig. 3, we actually multiplied $1.15^{-2/3} \sim 0.91$ to the noise curve of TianQin.

4 EXPECTED DETECTIONS

In this section, we estimate the expected numbers of detectable BBHs with the proposed space interferometers.

4.1 one component model

We first discuss a simple model with the single chirp mass $\mathcal{M} = \mathcal{M}_{10/3} = 15.5M_\odot$ and the comoving merger rate R at $R_0 = 19.1\text{Gpc}^{-3}\text{yr}^{-1}$. As explained later in the next subsection, by choosing this weighted average of the chirp masses, we can well reproduce the low frequency profile obtained by a more detailed analysis including the chirp mass spectrum.

The expected detection number $dN/d\ln f_i$ per logarithmic frequency interval is evaluated as

$$\frac{dN}{d\ln f_i} = V(f_i, T) \frac{dn}{d\ln f_i}, \quad (24)$$

in terms of the effective volume $V(f_i, T)$ defined in Eq. (19)

and the frequency distribution of the BBHs $dn/d\ln f$. Using the continuity equation in the frequency space, we have

$$\begin{aligned} \frac{dn}{d\ln f} &= f \left(\frac{df}{dt} \right)^{-1} R = \frac{5c^5 R}{96\pi^{8/3} G^{5/3} \mathcal{M}^{5/3} f^{8/3}} \quad (25) \\ &= 2.3 \times 10^{-6} \text{Mpc}^{-3} \\ &\times \left(\frac{f}{10\text{mHz}} \right)^{-8/3} \left(\frac{\mathcal{M}}{15.5M_\odot} \right)^{-5/3} \left(\frac{R}{19.1\text{Gpc}^{-3}\text{yr}^{-1}} \right). \end{aligned} \quad (26)$$

In Fig. 4, we present our numerical results for the observational periods $T = 4$ and 10yr with LISA and TianQin. The merging time becomes $t_{\text{mer}} = 4$ and 10yr respectively at the initial frequencies $f_i = 25.0$ and 17.7mHz , as shown in Fig. 4. At initial frequencies f_i higher than these frequencies, the BBHs merge in observational periods T (Sesana 2016). These binaries are important for ground-based detectors, and we specifically call them by merging BBHs below and let N_{mer} denote their expected number. Note that, for the single mass model, we can make a clear identification of the merging BBHs in the frequency space, as in Fig. 4. This is one of the reasons we use this simplified model here.

We define N_{tot} as the total number of expected BBH detections obtained by integrating Eq. (24). Because of the difference of the optimal bands, the number of merging BBHs N_{mer} is larger for TianQin than LISA. However, the total numbers N_{tot} of the detectable BBHs are similar. Quantitatively, we have $N_{\text{tot}} \sim 2$ and ~ 9 for $T = 4\text{yr}$ and 10yr , respectively.

For LISA and the observational period $T = 10\text{yr}$, we also include the Galactic confusion noise spectrum and show the result with the thin solid curve in Fig. 4. We have a minor correction ($\sim 3\%$ for N_{tot}) only at the low frequency end. Below, we ignore the Galactic confusion noise.

At the low frequency regime, we have $t_{\text{mer}} \gg T$ and the integral I_7 can be approximately evaluated as

$$I_7(f_i, T) \simeq T \left(\frac{df}{dt} \right)_{f_i} \frac{f_i^{-7/3}}{(3/20)S(f_i)}. \quad (27)$$

We then have

$$\frac{dN}{d\ln f_i} \approx \frac{\pi^{1/3} U G^{10/3} \mathcal{M}^{10/3} R}{3^{1/2} 5^{1/2} c^7 \rho_{\text{thr}}^3} \frac{f_i^{-2/3} T^{3/2}}{[(3/20)S(f_i)]^{3/2}}, \quad (28)$$

corresponding to the monochromatic frequency approximation in paper 1. In Fig. 4, we present this expression with the dashed curves. As expected, they reproduce the thick solid curves well at $f_i \lesssim 10\text{mHz}$.

As shown in Fig. 4, most of the detectable BBHs have merger time shorter than $t_{\text{mer}} \lesssim 10^3\text{yr}$. Then, for $T \gtrsim 4\text{yr}$, their chirp rates $\dot{f}_i \sim f_i/t_{\text{mer}}$ are much larger than its measurement error $\Delta \dot{f}_i \sim \rho^{-1} T^{-2}$ (see e.g., Takahashi & Seto 2002; Toubiana et al. 2020). Therefore, by using the observed chirp masses and distances, we can safely distinguish extra-Galactic BBHs from numerous Galactic binaries.

4.2 weighted results

We now study the averaged results using Eq. (9) for the 62 BBHs. In Fig. 5, for $T = 10\text{yr}$, we compare the results obtained with the full weighting operation and the single mass

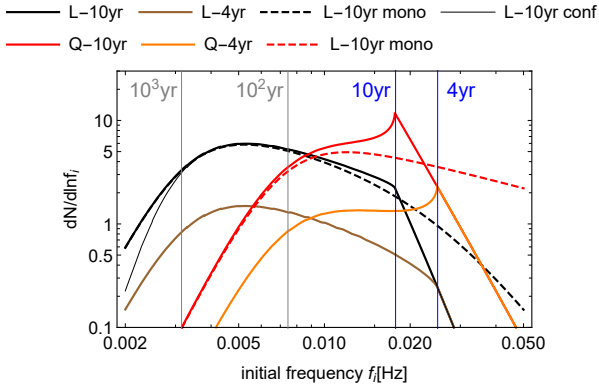


Figure 4. The expected number of BBH detections $dN/d\ln f_i$ per logarithmic initial frequency interval. We evaluated the simplified model with the single chirp mass $\mathcal{M} = 15.5M_\odot$ and the comoving merger rate $R = R_0 = 19.1\text{Gpc}^{-3}\text{yr}^{-1}$. The thick solid curves are for LISA and TianQin with observational periods $T = 4$ and 10yr. At frequencies f_i higher than the blue vertical lines, the BBHs merge in the observational periods T . The dashed curves are the monochromatic approximation (28) valid for $t_{\text{mer}} \gg T$. We include the Galactic confusion noise for the thin solid curve (LISA 10yr).

model in the previous subsection. We can see differences between them at $f_i \gtrsim 10\text{mHz}$ (corresponding to $t_{\text{mer}} = 10\text{yr}$ for $\mathcal{M} \sim 40M_\odot$).

Quantitatively, in the case of LISA, we have $(N_{\text{tot}}, N_{\text{mer}}) = (8.9, 0.83)$ for the weighted calculation and $(9.1, 0.34)$ for the single mass model. The relative magnitude of N_{mer} might look inconsistent with the two black curves in Fig. 5. However, we should notice that, for the weighted calculation, the number N_{mer} is dominated by heavier BBHs at the lower frequency range than the single mass model.

In Fig. 5, at $f_i \lesssim 7\text{mHz}$, the solid and dashed curves show reasonable agreement (less than 15% differences). In this regime, the monochromatic approximation works well, and we have $dN/d\ln f_i \propto R\mathcal{M}^{10/3}$ for the individual chirp masses as in Eq. (28). After the chirp mass weighting, we have $dN/d\ln f_i \propto R\langle\mathcal{M}^{10/3}\rangle = R(\bar{\mathcal{M}}_{10/3})^{10/3}$. Considering this relation, we have set $\mathcal{M} = \bar{\mathcal{M}}_{10/3} = 15.5M_\odot$ for the single mass model in the previous subsection.

In Fig. 6, we compare the cumulative chirp mass distributions for various weights of BBHs. Relative to the blue curve for the comoving merger rate (identical to the blue one in Fig. 2), those detected by LVKC (listed in GWTC-3) have the weight $\mathcal{M}^{5/2}$, as mentioned in §2. In fact, this should be regarded as the original observational data for our analysis. It has the identical vertical step of $1/62$. Under the monochromatic approximation (28), we have the stronger weight $\mathcal{M}^{10/3}$ for LISA. LISA is most likely to detect BBHs with $\mathcal{M} = 15 - 50M_\odot$, somewhat larger than the GWTC-3 samples. We should notice that this mass range is higher than the weighted result $\bar{\mathcal{M}}_{10/3} = 15.5M_\odot$, partly due to the nonlinearity of the operation (11). At present, reflecting the limited number of the GWTC-3 samples, the higher mass end $\mathcal{M} \gtrsim 50M_\odot$ has a large statistical uncertainty, also indicated by the comparison with the solid curves. In the stellar mass BBHs detected by LISA, a certain fraction $\sim 15\%$ could have chirp masses in the range $50 - 70M_\odot$.

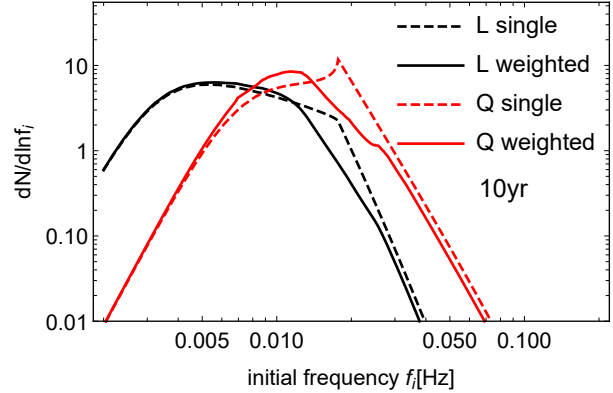


Figure 5. The comparison between the single mass calculation and the weighted results. At $f \lesssim 7\text{mHz}$, their differences are less than $\sim 15\%$.

In Fig. 5, at $f_i \gtrsim 30\text{mHz}$, we can see a small deviation between the solid and dashed curves. For these BBHs, we have $T > t_{\text{mer}}$ and the integral $I_7(f_i, T)$ becomes independent of the chirp mass [corresponding to $f_f = \infty$ in the integral (20)]. From Eq. (24), we then have $dN/d\ln f_i \propto R\mathcal{M}^{5/6}$ for the individual masses and $\propto R\langle\mathcal{M}^{5/6}\rangle = R(\bar{\mathcal{M}}_{5/6})^{5/6}$ after the weighting. Indeed, in Fig. 5, at $f_i \gtrsim 30\text{mHz}$, we find that the mismatch between the curves is a factor of $\sim (\bar{\mathcal{M}}_{5/6}/\bar{\mathcal{M}}_{10/3})^{5/6} = 0.7$.

Next we discuss dependence of the expected numbers $(N_{\text{tot}}, N_{\text{mer}})$ on the observational period T . The nominal operation period of LISA is 4 yr (Amaro-Seoane et al. 2017). In Fig. 7, we present our numerical results for LISA and TianQin. For $T = 4\text{yr}$, we have $(N_{\text{tot}}, N_{\text{mer}}) = (2.3, 0.10)$ with LISA and $(2.1, 0.61)$ with TianQin. We will have a fair chance to detect extra-Galactic BBHs with LISA, but they are not likely to merge in the observational period. TianQin has a larger chance to detect a merging BBH. At $T = 10\text{yr}$, we have $(N_{\text{tot}}, N_{\text{mer}}) = (8.9, 0.83)$ and $(7.8, 3.1)$, respectively, for LISA and TianQin. These numbers are basically consistent with the results of Liu et al. (2020).

As expected from Eq. (28), for LISA, the total number N_{tot} is approximately proportional to $T^{3/2}$. Meanwhile we can approximately show that $N_{\text{mer}} \propto f_i(T)^{-14/3} \propto T^{7/4}$, ignoring the frequency dependence of the noise spectrum. As expected from Fig. 3, this approximation works better for TianQin.

In any case, the expected numbers become much smaller than paper 1. For LISA, the detection number N_{tot} is dominated by nearly monochromatic BBHs and proportional to the product $R(\bar{\mathcal{M}}_{10/3})^{10/3}$. Comparing with paper 1, the product now becomes smaller by a factor of $(19.1/100)(15.5/28.6)^{10/3} = 0.025$. While the current target sensitivity of LISA is better than some of these examined in paper 1, the renewal of the astronomical information significantly reduced the expected numbers.

4.3 joint operation

Considering the timeline of the proposed missions such as LISA, Taiji and TianQin, we can expect their joint signal analysis. In this section, we discuss how the BBH detection could be improved by the coherent matched filtering anal-

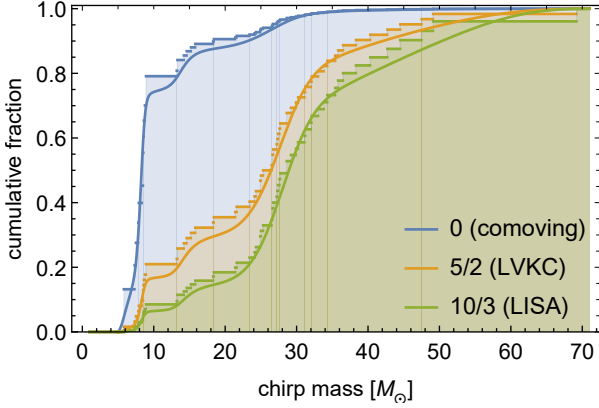


Figure 6. The cumulative chirp mass distributions for various weights of BBHs. Relative to the comoving merger rate, the LVKC detection (listed in GWTC-3) has the weight $\propto \mathcal{M}^{5/2}$ and the LISA detection has $\propto \mathcal{M}^{10/3}$ under the monochromatic approximation. The solid curves are obtained with the FM model prediction in Abbott et al. (2021b).

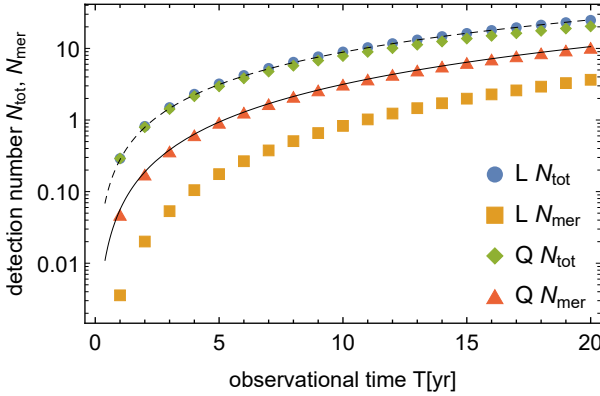


Figure 7. The expected detection numbers N_{tot} and N_{mer} for LISA and TianQin as functions of the observational periods T (after weighting). The dashed and solid curves are proportional to $T^{3/2}$ and $T^{7/4}$.

ysis (see also Liu et al. 2020). We specifically examine the following potential combinations of two 10yr-missions

- (i) L2-10: two LISA-equivalent detectors operated concurrently for 10 years (100% time overlap),
- (ii) L2-20: two LISA-equivalent detectors operated in a sequential order for a total of 20 years (0% time overlap),
- (iii) LQ-10: LISA and TianQin operated concurrently for 10 years (100% time overlap).

For L2-10 and L2-20, we imagine collaboration of LISA and Taiji (ignoring the difference of their noise spectra). For evaluating the total signal-to-noise ratio of the coherent analysis, we simply added the frequency integrals I_7 .

In Fig. 8, we present the frequency distributions $dN/d\ln f_i$ for the three combinations, together with the previous results for LISA (L-10) and TianQin (Q-10). We can see the asymptotic convergences for the two pairs (LQ-10, L-10) and (L2-10, L2-20) at the low frequency regime, and similarly (Q-10, LQ-10) at the high frequency regime. We can easily understand these behaviors, considering the optimal bands of detectors and the scaling relation of the monochromatic approximation (28). The asymptotic convergence is

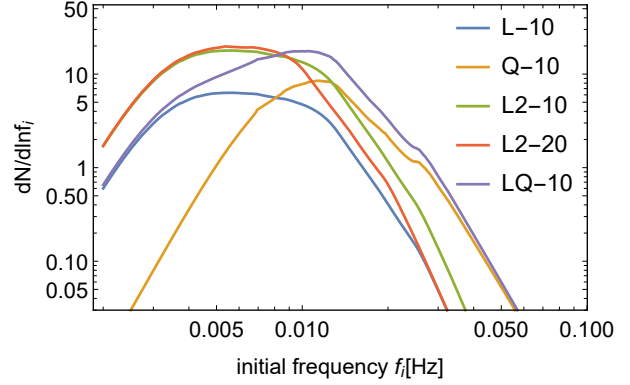


Figure 8. Results for the joint operations of space missions (see the main text for details of the five cases).

Table 1. The total detection numbers N_{tot} for the baseline operations (L-10 and Q-10), and the joint operations (L2-10, L2-20 and LQ-10). We also show the number of detectable BBHs N_{mer} with the merger time t_{mer} less than 10 and 20yr.

	L-10	Q-10	L2-10	L2-20	LQ-10
N_{tot}	8.9	7.8	25.3	24.7	22.2
$N_{\text{mer}} (t_{\text{mer}} < 10\text{yr})$	0.83	3.1	2.3	0.83	5.2
$N_{\text{mer}} (t_{\text{mer}} < 20\text{yr})$	2.1	5.2	5.9	3.6	9.9

also observed for (L-10, L2-20) at the high frequency regime, because all the binaries merge within 10yr.

In Table 1, we show the total number N_{tot} at the end of the operations. For the three networks L2-10, L2-20 and LQ-10, we have $N_{\text{tot}} \sim 20$ that is $2^{3/2} \sim 3$ times larger than L-10 and Q-10. In Table 1, we also present the number of merging BBHs N_{mer} with the remaining times $t_{\text{mer}} < 10\text{yr}$ and 20yr (slightly expanding the definition of N_{mer}). We should recall that the time t_{mer} is defined with the initial frequency f_i at the the beginning of the observation [see Eq. (14)]. If the results are compared at the same time span for $t_{\text{mer}} < 20\text{yr}$, L2-10 has larger numbers of ($N_{\text{tot}}, N_{\text{mer}}$) than L2-20. Thus, the coincident operation is more advantageous than the sequential operation for detecting stellar-mass BBHs. The coincident operation is also beneficial for sky localization of merging massive black hole binaries (see e.g., Ruan et al. 2018; Wang et al. 2020) and for correlation analysis of stochastic backgrounds (see e.g., Seto 2020).

5 DISCUSSIONS

So far, we have discussed BBH detection with space interferometers, setting the threshold at $\rho_{\text{thr}} = 10$. In reality, for a fixed chirp mass, we generally need a larger number of templates to find BBHs with space interferometers than ground based ones. Therefore, the required threshold ρ_{thr} would be higher for the former and could be $\rho_{\text{thr}} \sim 15$ (Moore et al. 2019). If we simply put $\rho_{\text{thr}} = 15$ (ignoring the frequency dependence) instead of 10, the detection numbers are reduced by a factor of $(15/10)^{-3} \sim 0.3$ from our estimation. Meanwhile, we should also notice that ground based interferometers will be able to detect the same BBHs later at higher signal-to-noise ratios. Thus, with multi-band obser-

vations for merging BBHs, we can decrease the threshold ρ_{thr} for space interferometers (Wong et al. 2018).

For the spatial distribution of BBHs, we have assumed a smooth extra-Galactic component. However, at the lower frequency regime (e.g., $f \sim 1\text{mHz}$), the detectable distances become smaller, and we might need to evaluate BBHs in our local group (e.g., Seto 2016). Unfortunately, at present, we observationally know little about the merger rate and chirp mass spectrum in the local group (see also Lamberts et al. 2018; Wagg et al. 2021).

We have also assumed that BBHs have circular orbits. Our results will be modified only slightly for small residual eccentricities, e.g., $e \sim 0.05$ at 5mHz (Nishizawa et al. 2017). However, the detectable numbers could be largely changed, if the BBHs typically have higher eccentricities e.g., $e \sim 0.5$ in the LISA band (see also Breivik et al. 2016; Samsing & D’Orazio 2018; Chen & Amaro-Seoane 2017).

6 SUMMARY

In this paper, we updated the prospects of extra-Galactic BBH search with space interferometers such as LISA and TianQin. We used the recent catalog GWTC-3 (Abbott et al. 2021b), targeting BBHs with component masses around $5\text{--}100M_{\odot}$ (and chirp masses $5\text{--}70M_{\odot}$). We directly incorporated the chirp masses distribution of the 62 BBHs detected at high significance.

For LISA, the total BBH detections are estimated to be $N_{\text{tot}} \sim 2(T/4\text{yr})^{3/2}(\rho_{\text{thr}}/10)^{-3}$ with the detection threshold ρ_{thr} . LISA detection will be dominated by nearly monochromatic BBHs in the mass range $\mathcal{M} = 15\text{--}50M_{\odot}$ with relatively large uncertainties above $50M_{\odot}$. As for the dependence on astronomical information, we have the scaling relation $N_{\text{tot}} \propto R(\bar{\mathcal{M}}_{10/3})^{10/3}$ with the comoving merger rate R and an weighted average of the chirp masses $\bar{\mathcal{M}}_{10/3}$. Compared with our previous estimation shortly after announcement of GW150914, the product $N_{\text{tot}} \propto R(\bar{\mathcal{M}}_{10/3})^{10/3}$ is reduced by a factor of $\sim 1/40$ [$\sim 1/5$ from R and $\sim 1/8$ from $(\bar{\mathcal{M}}_{10/3})^{10/3}$].

The Chinese project TianQin will have a total detection number N_{tot} similar to LISA. Meanwhile, it has potential to find $N_{\text{mer}} \sim 0.6(T/4\text{yr})^{7/4}(\rho_{\text{thr}}/10)^{-3}$ BBHs that merge in the observational period T . Because of the difference of the optimal bands, LISA will have 4-5 times smaller N_{mer} . Therefore, during its nominal operation period $T \sim 4\text{yr}$, LISA alone is not likely to detect any merging stellar-mass BBH, even optimistically counting an uncertainty factor of ~ 2 for the overall comoving merger rate. A longer operation period and joint data analysis with other detectors can largely improve the prospects for the detection.

ACKNOWLEDGEMENTS

This work is supported by JSPS Kakenhi Grant-in-Aid for Scientific Research (Nos. 17H06358, 18H05236, 19K03870, 19K14720 and 20H00158).

REFERENCES

- Abbott B. P., Abbott R., Abbott T. D., Abernathy M. R., Acernese F., Ackley K., Adams C., et al., 2016, *PhRvL*, 116, 061102. doi:10.1103/PhysRevLett.116.061102
- Abbott R., Abbott T. D., Acernese F., Ackley K., et al., 2021a, arXiv, arXiv:2111.03606
- Abbott R., Abbott T. D., Acernese F., Ackley K., et al., 2021b, arXiv, arXiv:2111.03634
- Amaro-Seoane P., Audley H., Babak S., Baker J., Barausse E., Bender P., Berti E., et al., 2017, arXiv, arXiv:1702.00786
- Chen X., Amaro-Seoane P., 2017, *ApJL*, 842, L2. doi:10.3847/2041-8213/aa74ce
- Breivik K., Rodriguez C. L., Larson S. L., Kalogera V., Rasio F. A., 2016, *ApJL*, 830, L18. doi:10.3847/2041-8205/830/1/L18
- Del Pozzo W., Sesana A., Klein A., 2018, *MNRAS*, 475, 3485. doi:10.1093/mnras/sty057
- Huang S.-J., Hu Y.-M., Korol V., Li P.-C., Liang Z.-C., Lu Y., Wang H.-T., et al., 2020, *PhRvD*, 102, 063021. doi:10.1103/PhysRevD.102.063021
- Isoyama S., Nakano H., Nakamura T., 2018, *PTEP*, 2018, 073E01. doi:10.1093/ptep/pty078
- Kyutoku K., Seto N., 2016, *MNRAS*, 462, 2177. doi:10.1093/mnras/stw1767
- Lamberts A., Garrison-Kimmel S., Hopkins P. F., Quataert E., Bullock J. S., Faucher-Giguère C.-A., Wetzel A., et al., 2018, *MNRAS*, 480, 2704. doi:10.1093/mnras/sty2035
- Liu S., Hu Y.-M., Zhang J.-. dong ., Mei J., 2020, *PhRvD*, 101, 103027. doi:10.1103/PhysRevD.101.103027
- Luo J., Chen L.-S., Duan H.-Z., Gong Y.-G., Hu S., Ji J., Liu Q., et al., 2016, *CQGra*, 33, 035010. doi:10.1088/0264-9381/33/3/035010
- Moore C. J., Gerosa D., Klein A., 2019, *MNRAS*, 488, L94. doi:10.1093/mnras/512/1/l94
- Nair R., Jhingan S., Tanaka T., 2016, *PTEP*, 2016, 053E01. doi:10.1093/ptep/ptw043
- Nishizawa A., Sesana A., Berti E., Klein A., 2017, *MNRAS*, 465, 4375. doi:10.1093/mnras/stw2993
- Prince T. A., Tinto M., Larson S. L., Armstrong J. W., 2002, *PhRvD*, 66, 122002. doi:10.1103/PhysRevD.66.122002
- Robson T., Cornish N. J., Liu C., 2019, *CQGra*, 36, 105011. doi:10.1088/1361-6382/ab1101
- Ruan W.-H., Guo Z.-K., Cai R.-G., Zhang Y.-Z., 2018, arXiv, arXiv:1807.09495
- Samsing J., D’Orazio D. J., 2018, *MNRAS*, 481, 5445. doi:10.1093/mnras/sty2334
- Sesana A., 2016, *PhRvL*, 116, 231102. doi:10.1103/PhysRevLett.116.231102
- Seto N., 2014, *Phys. Rev. D*, 90, 027303
- Seto N., 2016, *Mon. Not. R. Astron. Soc.*, 460, L1
- Seto N., 2020, *PhRvD*, 102, 123547. doi:10.1103/PhysRevD.102.123547
- Takahashi R., Seto N., 2002, *Astrophys. J.*, 575, 1030
- Toubiana A., Marsat S., Babak S., Baker J., Dal Canton T., 2020, *PhRvD*, 102, 124037. doi:10.1103/PhysRevD.102.124037
- Wagg T., Broekgaarden F. S., de Mink S. E., van Son L. A. C., Frankel N., Justham S., 2021, arXiv, arXiv:2111.13704

Wang G., Ni W.-T., Han W.-B., Yang S.-C., Zhong X.-Y., 2020, *PhRvD*, 102, 024089.
doi:10.1103/PhysRevD.102.024089

Wong K. W. K., Kovetz E. D., Cutler C., Berti E., 2018, *PhRvL*, 121, 251102.
doi:10.1103/PhysRevLett.121.251102